Research Article | Vol. 27, No. 25 / 9 December 2019 / Optics Express 36524
Optics EXPRESS

Towards Poisson noise limited optical pump soft X-ray probe NEXAFS spectroscopy using a laser-produced plasma source

ADRIAN JONAS,[1,2,*] HOLGER STIEL,[1,3] LISA GLÖGGLER,[1,2] DIANA DAHM,[1,2] KATHARINA DAMMER,[1,2] BIRGIT KANNGIEßER,[1,2] AND IOANNA MANTOUVALOU[1,2]

[1]Berlin Laboratory for innovative X-ray technologies (BLiX), D-10623 Berlin, Germany
[2]TU Berlin, Analytical X-Ray Physics, D-10623 Berlin, Germany
[3]Max-Born-Institut für Nichtlineare Optik und Kurzzeitspektroskopie, D-12489 Berlin, Germany
*Adrian.Jonas@campus.tu-berlin.de

Abstract: We present a laboratory setup for near edge X-ray absorption spectroscopy (NEXAFS) in the soft X-ray regime between 284 eV to 1303 eV with a resolving power of up to 1370. Based on a laser-produced plasma source, a pair of identical reflection zone plates and an X-ray CCD camera, the setup is intended for optical pump X-ray probe NEXAFS measurements with a detectable change in absorption of the excited sample down to 10^{-4} and 500 ps time resolution. Because of the high stability of the source the statistical error only depends on the detector response and the number of photons detected and can reach the detector noise limit after a couple of thousands single shots. Thus, structure-function relationship investigations of bio-molecules are rendered feasible in the laboratory.

1. Introduction

Near edge X-ray absorptions fine structure (NEXAFS) spectroscopy is an analytical tool which yields information about the chemical surrounding of an atom. By observing the absorption of X-rays with high energy resolution in the region of an absorption edge, unoccupied states are probed and especially when using soft X-ray radiation, the electronic structure of molecular orbitals can be investigated.

NEXAFS is commonly carried out at synchrotron radiation facilities or free electron lasers were beamtime is limited. Therefore and due to the advent of suitable soft X-ray sources, laboratory based NEXAFS setups have been introduced more frequently in the last couple of years. Such setups are typically driven with high harmonic generation (HHG) [1–4] or laser produced plasma (LPP) [5–7] sources coupled with high resolution spectrometers.

HHG sources produce polarized, coherent light with ultra-short pulse lengths down to few hundreds of attoseconds, with the disadvantage, that the photon flux for photon energies higher than 500 eV decreases drastically. Nevertheless NEXAFS investigations up to the N K-edge have recently been demonstrated [8]. Using mid-infrared driving lasers for HHG even transition metal L-edges are accessible [2]. However, due to the relatively low photon flux statistics of the reported spectra are rather low. For the measured N K-edge data reported in [8] a signal-to-noise ratio (SNR) below 10 can be estimated. LPP sources on the other hand reach much higher photon flux while working at longer timescales. Different groups have shown successful LPP NEXAFS measurements above the N K-edge [9,10] which have already demonstrated the potential of the technique while not fully exploiting the possibilities concerning either high resolution or SNR.

An extension of static NEXAFS spectroscopy is optical pump X-ray probe NEXAFS (pp-NEXAFS) spectroscopy where the photo-induced dynamics of the electronic structure of a given sample is analyzed. Thereby, additional information compared to static measurements

#369498 https://doi.org/10.1364/OE.27.036524
Journal © 2019 Received 6 Jun 2019; revised 12 Sep 2019; accepted 13 Sep 2019; published 2 Dec 2019

Optics EXPRESS

is accessible rendering the understanding of structure-function relationships in bio-molecular systems feasible. While pp-NEXAFS is an established method [11–14], it has gained increased popularity only recently [15–18] due to advances in source and spectrometer design. This is especially true for soft X-ray pp-NEXAFS [19–21]. Pp-NEXAFS demands on the setup in respect to energy resolution and SNR are high, as the induced absorption changes (ΔA) and/or spectral shifts can be very small. Depending on the sample, sample environment, pump pulse duration and time delay typical differences ΔA are in the range of $2{\cdot}10^{-1}$ to $5{\cdot}10^{-2}$ [19,22], although values smaller than 10^{-3} can occur [23]. Energetic shifts lie in the meV range [11]. Thus, highly efficient and stable setups are mandatory.

We present an optimized setup for soft X-ray NEXAFS spectroscopy in the laboratory with high spectral resolution, stability and efficiency. Adapted data acquisition modes and data analysis lead to a maximal flexibility of the setup for investigations at photon energies starting at the C K-edge up to rare earths M-edges. The performance of the setup for NEXAFS spectroscopy is shown exemplary using thin foil samples demonstrating the comparability to state-of-the-art setups at synchrotron radiation facilities. Finally, characterization measurements regarding the statistical error of a pp-NEXAFS measurement are shown.

2. Experimental

The NEXAFS spectrometer is based on the design already presented in [27], where the polychromatic, isotropic, pulsed soft X-ray radiation from a LPP source [25,26] is used for scanning free X-ray absorption experiments in transmission mode [5]. In contrast to setups where the energy is scanned, the absorption A is measured by the simultaneous collection of the whole sample and reference spectra with dispersing optics and calculating the natural logarithm of the ratio of the two. This collection is facilitated with off-axis reflection zone plates (RZP; Nano Optics Berlin GmbH) and an X-ray CCD camera sensor (Greateyes GmbH, GE 2048).

The major advancement in the current setup is the use of identical pairs of RZP structures and a larger CCD camera, enabling the detection of reference and sample spectrum simultaneously. Additionally, an attached pinhole camera provides source position and size for each shot. In the following the different components are described in detail focusing on the changes in the optimized setup.

A schematic view of the setup is depicted in Fig. 1. A powerful Yb:YAG thin disk laser (1030 nm, ≤ 200 mJ pulse energy, 100 Hz repetition rate) is focused onto a rotating solid copper cylinder to produce a continuous soft X-ray spectrum in the range of 100 eV to 1600 eV. Different foils can be taped onto the copper cylinder to change the plasma emission spectrum with tungsten foil used as the standard material for a quasi-continuous spectrum [5]. The surface of the cylinder can be used for approximately 2 million shots (13 h @ 100 Hz) before servicing. The used tungsten foil (0.1 mm · 570 mm · 5 mm, HMW Hauner GmbH & Co. KG) covers half of the cylinder. Low to medium Z plasma targets like Cu produce isolated characteristic lines in the emission spectrum which are beneficial for energy calibration, but may introduce artifacts in the absorption spectrum. High Z targets produce quasi-continuous spectra with typically higher flux resulting in shorter recording times. Due to a temperature gradient in the expanding plasma the source size as seen by the spectrometer is different for different photon energies. An average value over the whole energy range using the copper target yields a FWHM in the range of ~50 µm. In comparison to [27] the pulse duration of the laser and consequently also the X-ray pulse duration can be continuously tuned between 500 ps and 30 ns.

The soft X-rays are emitted isotropically and are transmitted through the sample and reference, with the reference most commonly being silicon nitride (Si_3N_4) windows which act as the support for the transmission samples. The standard window size is 2·2 mm⊃2 with a thickness of 150 nm. The sample chamber has a manual linear feedthrough to adjust the height of the whole sample stage. The horizontal position of both windows can be adjusted individually using two in-vacuum

Optics EXPRESS

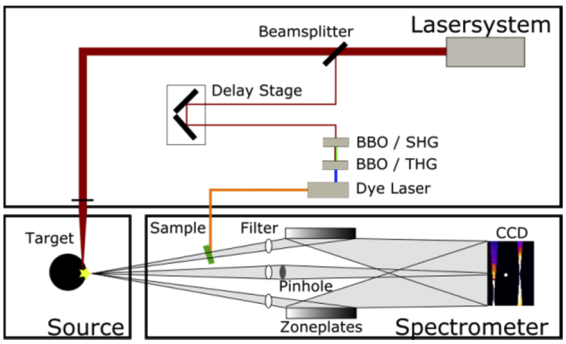

Fig. 1. Schematic view of the setup with laser system and pump beamline (top), source and spectrometer (bottom).

motorized stages. The sample window is positioned 64 cm behind the source. Depending on the investigated sample, filters can be inserted for debris protection. Due to the large source-sample distance even without filters, NEXAFS measurements can be conducted for about 20 000 shots before contamination becomes noticeable. Scattered laser light and the visual part of the plasma spectrum are blocked using free standing XUV filter foils placed behind the sample chamber. For measurements at absorption edges lower than 450 eV a 200 nm thin titanium filter and for energies above 450 eV a 200 nm Al filter is used. Transmitted X-rays are dispersed by the RZP's situated 150 cm after the source spot. The incidence angle at the design energy of the RZP's is 2° and the refraction angle is 3.66°. Each optical mounts consist of a motorized stage with 4 motors (2 translational and 2 rotational) and can hold 4 RZP's simultaneously. The RZP's are designed for different focus energies, see Table 1 and can be selected by moving the stage in vertical direction. Horizontal translation perpendicular to the optical axis as well as the rotation in the meridional and sagittal plane are needed to adjust the RZP. The movement of the motors of the four different RZP structures is sufficient to align the optics to any photon energy emitted by the source through misalignment [24] thus, enabling NEXAFS spectroscopy of all existing absorption edges between 284 eV (C K-edge) and 1303 eV (Mg K-edge). The sample and reference spectra are collected by an X-ray CCD 250 cm behind the RZP's. A pinhole camera is installed along the optical axis between the two X-ray beams paths. Therefore, each CCD frame contains the sample and reference spectrum as well as an image of the source. The diameter of the pinhole is 50 µm, the object and image distances are 140 cm and 260 cm. In front of the pinhole a 200 nm thick Al foil is used to filter visible light and to restrict the photon energy range seen by the pinhole camera.

Table 1. Parameters of the used RZP structures

Structure	Absorption edge	Energie / eV	Size / mm^2
1	C K-edge	284	20×80
2	N K-edge	410	15×80
3	O K-edge	543	10×80
4	Cu L_3-edge	933	10×80
5	Mg K-edge	1303	10×80

The back illuminated CCD has a pixel size of 13.5·13.5 µm⊃2 and is cooled down to −30°C. To reduce the read out time, detector noise and data size the CCD is usually binned 8-fold in vertical direction reducing the amount of pixels to 2048·256. Higher binning values cannot be used either because of saturation of the CCD or online data evaluation speed. The whole

Optics EXPRESS

spectrometer consisting of plasma chamber and spectrometer divided by a gate valve is under high vacuum conditions (10^{-7} mbar). The whole setup has a footprint of about 3 m·4.5 m.

The cylindrical target is rotated after each laser shot in order to assure a fresh target surface, which leads to a slight change in target position. Without correction the source spot travels in a sinusoidal movement with an amplitude of about 50 µm during one full rotation. Due to its slitless design the RZP spectrometer setup is sensitive to such changes resulting in a change of resolving power and spectrum positioning on the CCD camera. In so called continuous mode (at full repetition rate of the thin disk laser), a target correction system using a pinhole camera attached to the plasma chamber as described in [26] reduces this source movement to a drift of about 5 µm. Due to the high efficiency of the spectrometer setup, single shot images often already utilize the whole dynamic range of the CCD camera. Therefore the continuous mode correction method cannot be used routinely for data acquisition because the frame rate of conventional CCD cameras is much lower than the repetition rate (100 Hz) of the source. A new standard single shot mode (SSM) is introduced which will be described in the following. Using SSM, one NEXAFS spectrum is obtained with one shot of the source and a certain number of spectra are collected. Experimentally to obtain a SSM image, a fast single blade shutter is inserted in the laser system between seed diode and regenerative amplifier which opens for < 10 ms so that a maximum of one pulse can pass. The shutter is controlled by the CCD camera. After each picture is taken the source spot on the CCD is evaluated with a 2D Gaussian fit yielding an (x,y) position of the spot. Here x is the dispersion direction and y perpendicular to x. Because of the geometry the spot on the CCD is more prone to changes in the y direction. The standard deviation of the source position in x direction amounts to less than 5 µm. For the y-position it reaches a maximum of 60 µm for taped foils such as tungsten and 50 µm for the bare copper cylinder. As the position of the source moves in a slow sinusoidal fashion, this movement can be corrected with a target correction motor which moves the cylinder in vertical direction, see Ref. [26] for details. Such a correction was implemented resulting in a standard deviation of the y position of 13 µm. Absolute shifts of the spectrum are dealt with in the data evaluation.

Due to the use of different RZP structures the energy resolution of the spectrometer is in first approximation independent on the absorption edge energy and designed to be theoretically $E/\Delta E = 1750$ for a source size of 35 µm. In practice this value is limited to 900–1500 by the energy dependent source size and the charge cloud size of the CCD detector. Using two optical elements instead of one introduces additional differences in sample and reference spectrum as they are collected with two different RZP's and filters. For quantification differences in reflectivity of the RZP's and filter transmission can be accounted for with characterization measurements as they do not change with time. Generally, such systematic errors are below 5% (~0.05 A). For pump probe spectroscopy in general this is not necessary because the difference cancels out.

For pump probe spectroscopy a small part of the laser pulse is separated using a beam splitter consisting of a $\lambda/2$-plate and a thin film polarizer. This guaranties that there is no time jitter between pump and probe pulse. The intensity of the pump and probe beam can be adjusted using the $\lambda/2$ plate and the current for the pump diodes of the laser system. The wavelength of the pump pulse can be tailored using a pair of nonlinear crystals and/or a dye laser. The first BBO crystal produces the 2nd harmonic (515 nm) of the laser and the second BBO generates the 3rd harmonic (343 nm) by adding the 1st and 2nd harmonic. The 2nd or 3rd harmonic can be used as pump for a dye laser that can be tuned between 400 nm and 900 nm, depending on the dye. With the current 40 cm long linear stage the time delay between pump and probe pulse can be manually adjusted between 0 and 2.7 ns. Longer time delays are possible by extending the pump beam path. To eliminate possible long time instabilities of the laser or detector, the measurement mode is implemented in such a way, that static and pumped NEXAFS images are collected alternating.

Optics EXPRESS

2.1. Data evaluation

The data evaluation is automated using a routine written in Python. For most measurements a couple of hundred or thousand SSM images are taken. Each CCD image is processed individually. A section of 50 averaged CCD images taken with a TiO_2 sample is shown in Fig. 2.

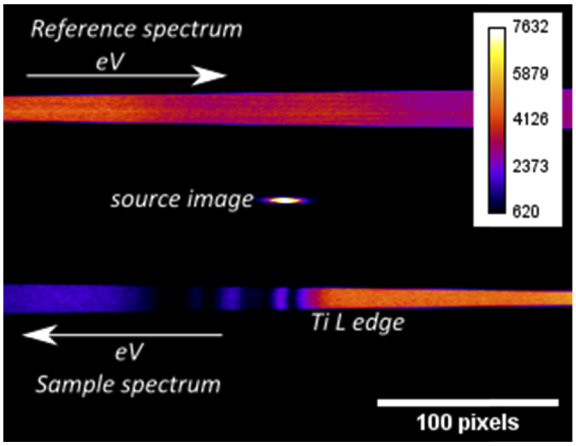

Fig. 2. Detail of 50 averaged SSM images with the reference (top) and sample (bottom) spectrum as well as the image of the source (middle) using tungsten as source material and 1 ns pulse duration. The pixels are binned 8x in vertical direction. The Ti L-edge absorption is clearly visible in the sample spectrum.

To acquire the NEXAFS spectrum from the CCD image the background is subtracted. The parts containing the source image, the reference and sample signal are cropped. The source image is evaluated using a 2D Gaussian intensity distribution in order to monitor the stability and size of the source. To obtain the reference and sample spectra the counts in each pixel column of the cropped parts are summed up. Because the RZP's are facing each other the reference and sample spectra are mirrored. Therefore the sample spectrum is flipped and then shifted onto the reference spectrum energy axis. To improve the accuracy of this shifting process the spectra are interpolated by a factor of 10 using a cubic spline. According to the Lambert-Beer law the absorption A is obtained by the natural logarithm of the reference spectra R(E) divided by the sample spectra S(E):

$$A(E) = \ln\frac{R(E)}{S(E)}. \tag{1}$$

During the collection of multiple images the source position slightly changes in x- and y-direction (see above). The change in y-direction can be disregarded because of the summation of each pixel column without any drawbacks. The change in x-direction is accounted for by shifting the individual NEXAFS spectra before averaging which results in a 10% enhancement of energy resolution. The energy axis is calibrated using tabulated atomic emission lines of the copper plasma emission reference spectrum. This procedure is described in detail in [25]. The absolute photon energy value can be determined with an uncertainty of 0.2 eV – 0.5 eV depending on the existence and accuracy of tabulated atomic emission lines. Each summed pixel column forms an energy channel with an energy dependent width between 0.06 eV (C K-edge) and 0.4 eV (Mg K-edge)

Using a grating based diffraction optic, an enhanced field of depth can be achieved by introducing an aperture such as a pinhole, slit or blade [24]. In our setup the sample and reference windows can be used as an aperture. By moving the windows out of the collected solid angle of the RZP's in direction of dispersion one can increase the depth of field continuously. At the

Optics EXPRESS

same rate the collected solid angle of the RZP decreases and therefore the number of collected photons per image. Also the effective illuminated sample width is reduced and the sample is only measured at one of its edges. This can be harmful for inhomogeneous samples and increases the measuring time by a factor of 5–10. If the sample width is smaller than 200 µm the depth of field is always high enough to cover more than 200 eV in one spectrum.

3. Results: NEXAFS spectra of transition metal samples

3.1. Preparation of anatase samples

Two anatase films were prepared in the following way. The anatase nanoparticle paste 18NR-T (greatcellsolar) with a concentration of 0.12 g/ml in ethanol was deposited on a Si_3N_4 membrane (150 nm thickness, 2×2mm⊃2 area) using a spincoater with 960 rmp. The sample was heated afterwards for 30 minutes and 280°C to remove carbon residues in the paste. For the first sample this process was repeated three times resulting in a thin homogenous TiO_2 film with a thickness of 150 ± 30 nm. For the second sample it was repeated two times resulting in a 100 ± 20 nm thick film.

3.2. NEXAFS spectra of transition metal samples

Figure 3 (top left) shows the TiO_2 Ti L-edge NEXAFS spectrum of the 150 nm thick film. The spectrum is the average of 1500 SSM spectra. Additionally a NEXAFS spectrum obtained using only a single shot is depicted in red with in offset.

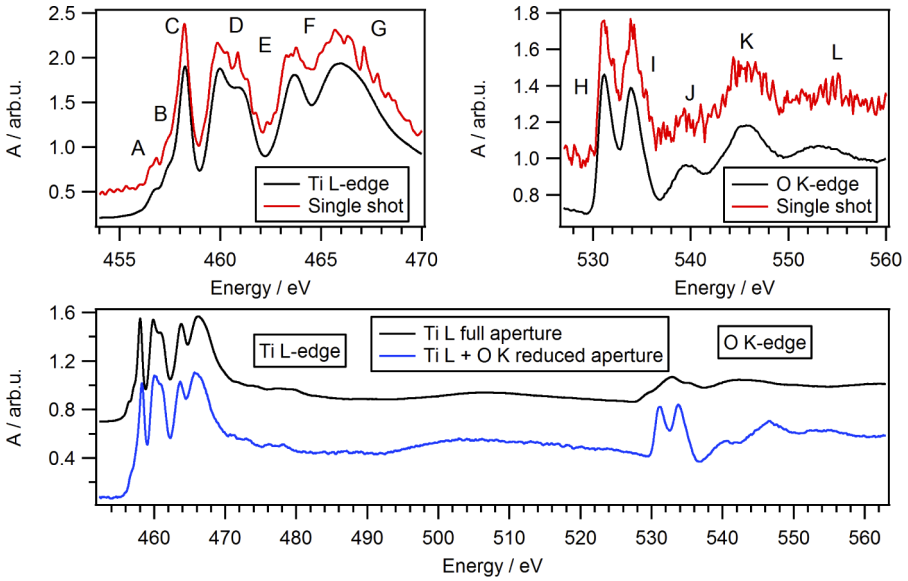

Fig. 3. Ti L and O K absorption edges of a 150 nm thick TiO_2 sample using 1500 and 300 SSM images, respectively (top) Bottom: a spectrum containing both edges of a 100 nm TiO_2 sample using 2000 SSM images (blue).

Features A-G are well known from literature [28,29,30] and clearly resolved in the spectrum of Fig. 3 (top left), see Table 2. The pre-edge features A and B origin in multiplet core hole – d electron interactions [30]. The L_3 and L_2-edges (features C-G) correspond to transitions from the Ti 2 $p_{3/2}$ and Ti 2 $p_{1/2}$ orbitals into the 3d orbitals. Due to the octahedral geometry of anatase the 3d orbitals (L_2 and L_3-edges) of Ti divide into two sets of different energies (crystal field

Optics EXPRESS

splitting) corresponding to t_{2g} and e_g symmetry. Additionally the upper 3d e_g level at the L_3-edge (features D, E) splits due to distortion of the coordination environment [29].

Table 2. Features in the Ti L and O K absorption spectra with reference values for the measurements presented in Fig. 3.

Features Ti L	This work Energy in eV	Reference [4] Energy ± 0.1 in eV	Features O K	This work Energy in eV	Reference [6] Energy in eV
A	456.7 ± 0.2	456.7 ± 0.1	H	531.2 ± 0.2	531.3
B	457.5 ± 0.2	457.4 ± 0.1	I	534.0 ± 0.2	534.0
C	458.2 ± 0.2	458.3 ± 0.1	J	539.6 ± 0.2	539.3
D	459.9 ± 0.2	460.1 ± 0.1	K	545.2 ± 0.2	544.8
E	461.0 ± 0.2	460.9 ± 0.1	L	554	555
F	463.5 ± 0.2	463.7 ± 0.1			
G	465.9 ± 0.2	465.7 ± 0.1			

Figure 3 (top right) shows a measurement of the same sample at the O K-edge. 300 SSM spectra have been averaged. Again the first two features originate from transitions into the t_{2g} and e_g orbital [32]. Features J, K and L are transitions from the O 1*s* orbital into the covalent mixed O 2*p* and Ti 4*sp* orbitals [31,33].

The accuracy of the measurement is equal to the standard deviation of the pre-edge region. In the pre-edge region the noise level of the single shot NEXAFS is $3{\cdot}10^{-2}$ and $9{\cdot}10^{-4}$ for the averaged spectrum following the Poisson limited $1/\sqrt{n}$ dependency where n is the number of recorded SSM spectra. The resolving power of this measurement was determined to be 970 ± 10 using the FWHM of the atomic emission line of copper at 457.9 eV. For the O K-edge spectrum in Fig. 3 (top right) the single shot spectrum has been measured with an accuracy ΔA of $4{\cdot}10^{-2}$ in the pre-edge region while for the averaged spectrum this value was determined to be $3{\cdot}10^{-3}$. In Fig. 3 (bottom) the Oxygen K-edge and Ti L-edge of the second sample (d = 100 nm) was measured at the same time using the O K RZP structure with 2000 SSM images (blue). To measure with high resolution at both the Ti L-edge and O K-edge the vertical aperture has to be reduced by a factor of 5–10 [24]. For comparison the Ti L-edge measurement is shown in black with an offset. Here, the decrease of energy resolution is clearly noticeable at the O K-edge. The noise of the black spectrum is visibly higher in comparison to Fig. 3 (top) due to the smaller aperture and thinner sample. Additionally, differences in structure height ratio can be discerned, which are in part explained by the use of two different samples and in part due to energy resolution effects. While in the case of Fig. 3 (top) the maximal energy resolution was aligned to the two respective edges, in Fig. 3 (bottom) the highest energy resolution lies somewhere between the two edges and decreases slightly but noticeably towards higher and lower focus energies [27].

To demonstrate the capability of the setup for NEXAFS measurements at higher photon energies, two experiments at the copper L-edge and magnesium K-edge were performed, see Fig. 4. For the Cu L-edge a 200 nm thick metallic copper foil was used as sample. 2000 SSM images were taken and averaged. The pre-edge region shows a standard deviation of $3{\cdot}10^{-3}$. To explore the limits of the current setup investigations at photon energies up to 1303 eV have been accomplished. Due to the relevance of magnesium as central metal atom in photosynthetic pigments [36] a 3 µm thick Mg foil has been chosen as sample subject. The Mg K-edge at around 1303 eV is at the high energy end of the LPP emission spectrum with 3 orders on magnitude less photons per energy channel compared to the C K-edge. Therefore, Mg K-edge was measured in continuous mode. 15 images with an exposure time of 15 s (1500 shots) were taken and averaged. The general shape of the NEXAFS and oscillations in the extended X-ray absorption fine structure (EXAFS) are visible but the noise is much higher than that of other measurements. To improve the visibility of the NEXAFS features the black line shows a smoothed spectrum using a 2nd

Optics EXPRESS

order 21 point Savitzky-Golay filter. The Mg K-edge is measured to be 1303.9 ± 0.2 eV which agrees with literature (1303.6 ± 0.7 eV) [36]. The standard deviation in the pre-edge region is $8{\cdot}10^{-3}$ in spite of accumulating 22500 shots. The standard deviation in the EXAFS region is $7{\cdot}10^{-2}$. For a standard deviation of under $1{\cdot}10^{-4}$ (pre-edge) or $1{\cdot}10^{-3}$ (EXAFS) an exposure time of about 4 hours in continuous mode would be needed. Both spectra in Fig. 4 can be calibrated with an uncertainty of about 0.2 eV using the copper plasma emission lines in the 0.9–1.3 keV region [27]. A maximum resolving power of 1370 ± 10 was achieved for the Cu L NEXAFS using the Cu plasma emission line at 950.5 eV and 1140 ± 10 for the Mg K-edge using the Cu plasma emission line at 1302.2 eV. The presented spectra in Fig. 3 and especially Fig. 4 show the high-end performance of the presented setup, which is comparable with state-of-the-art results obtained at synchrotron radiation facilities [28–36].

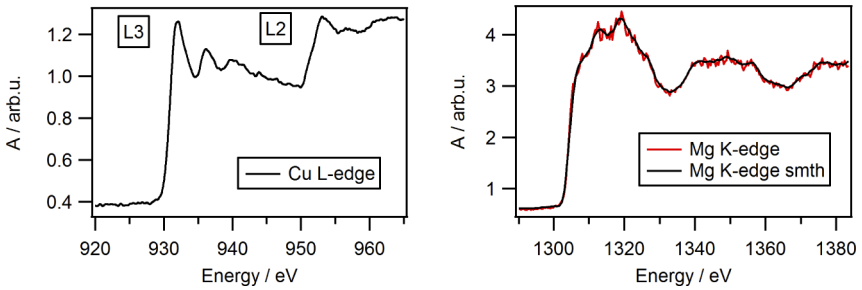

Fig. 4. Cu L-edge NEXAFS using a 200 nm Cu foil, 2000 SSM images (left); Mg K-edge NEXAFS of a 3 µm thick Mg foil measured in continuous mode with a total exposure time of 225 s (corresponding to 22500 shots) (right).

4. Statistical considerations concerning pp-NEXAFS

The presented quality of the spectra is the prerequisite for pp-NEXAFS investigations as the changes of A in the NEXAFS spectra due to optical pumping can be very small ($\sim 10^{-4}$) and must be distinguished reliably for serious analytical investigations. To evaluate if the detection of such small differences with a specific setup is feasible, the statistical uncertainties have to be assessed, yielding the minimum number of SSM images necessary for a specific measurement. For this purpose the possible noise contributions and their influence on ΔA are described in the following.

There are only three contributions to the statistical error ΔA of a NEXAFS measurement using the spectrometer setup described above, the photon shot noise n_{ph}, the dark noise n_d and the readout noise n_{ro} of the detector. Following the error propagation of the Lambert-Beer law, the statistical error can be described by:

$$\Delta A(E) = \frac{\sqrt{e^A + 1}}{\sqrt{n_{ph}^2(E) + n_d^2 + n_{ro}^2}} \tag{2}$$

The detector dark noise n_d arises from thermally generated electrons within the CCD sensor. It depends on the CCD sensor temperature and exposure time. Cooling the CCD and using exposure times of a couple milliseconds, the detector dark noise is in the range of < 0.005 ph/channel and therefore negligible.

The photon shot noise n_{ph} arises from the inherent statistical nature of photons. It follows the Poisson distribution and is limited by the brightness of the source and the efficiency of the spectrometer. Both parameters are energy dependent. If N_{Ph} is the number of photons in one energy channel the photon shot noise n_{ph} is the square root of N_{Ph}. This statistical error is reduced by measuring multiple times. Depending on the used filter, RZP and photon energy 500–5000

Optics EXPRESS

photons/(channel·SSM image) are collected in the reference spectrum. Generally, an increase in the number of SSM images reduces n_{ph} further following the square root dependency.

The signal on the CCD is measured in counts (cts) which are converted to photons using:

$$N_{Ph}(E) = \left(\frac{cts * 3.65\text{eV} * g}{E}\right) = n_{ph}^2(E) \tag{3}$$

with g the gain, $N_{Ph}(E)$ the number of photons and E the energy of one photon in eV. The factor 3.65 is the mean energy needed to create one electron hole pair in the silicon based detector. For the used CCD camera the gain is 2.5 as supplied by the manufacturer and validated by single photon event evaluation [37].

The detector readout noise n_{ro} originates from the process of converting the collected charge into voltage in every pixel. It is added to the signal in every image taken. This error source can only be reduced by pixel binning, slower readout speed and the use of the whole dynamic range of the detector. As it is a specific measure of the used CCD camera, an experimental determination in the spectrometer is advisable. At 1 MHz readout speed a read-out noise per pixel n_{ro_pixel} of 1.3 counts, or 1.6 counts (8x binning) was measured. Due to the summation of pixels in the data evaluation process, the contribution of the read out noise in every energy channel depends on the number of pixels N_{pixel} with noise n_{ro_pixel} summed. Therefore a minimization of N_{pixel} is desirable. The RZP structure focusses only radiation with the design energy onto the CCD. Other energies are broadened in the vertical direction, resulting in a cross shaped pattern on the CCD. In the focus region the spectrum is only 6 pixel high (FWHM) and correlates to the image of the source's height (50 µm). In the direction to lower or higher energies (horizontal) the spectrums height increases linearly. The height can reach over half of the CCD size i.e. 1000 pixel. This is only the case when the full solid angle of the C K RZP is used. When using standard 2·2 mm⊃2 Si_3N_4 windows as sample support, the solid angle of detection is reduced and only roughly 400 pixels are illuminated. This means summing over 400 pixels will give an overall read out noise in each channel of 26 counts. With 8x binning only 50 pixels are necessary to enclose the whole spectrum leading to a noise of only 11 counts. This value can be reduced further to about 4 counts, when only one absorption edge is of interest because in this case only about +−20 eV around the absorption edge is needed which renders the summation over only 5 pixels with 8x binning sufficient. Depending on photon energy, sample and number of photons per channel these 4 counts, convert into a noise level that cannot be undershot by accumulating measurements in SSM of $2{\cdot}10^{-4}$ (C K-edge), see Table 3.

Table 3. Typical parameters obtained with 120 mJ and 1 ns, 150 nm thick 2 mm·2 mm Si_3N_4 windows, W target.

RZP structure	C K-edge	N K-edge	O K-edge	Cu L-edge	Mg K-edge
Readout noise limit	$2{\cdot}10^{-4}$	$5{\cdot}10^{-5}$	$4{\cdot}10^{-5}$	$8{\cdot}10^{-5}$	$3{\cdot}10^{-2}$
Mean photons cts/channel	700	2000	2000	500	1
Filter / nm	Ti 200	Ti 200	Al 200	Al 200	Al 1500

As an example 500 images have been taken with the C K RZP structure and tungsten as target material. In Fig. 5 the energy/channel dependent standard deviation of those 500 SSM NEXAFS spectra is shown.

As sample and reference a standard 2·2 mm⊃2 x 150 nm Si_3N_4 window was used. For comparison the black dashed line shows the expected error derived from the measured sum spectrum assuming only Poisson statistics. The basic shape of the curve follows the inverse of the emission spectrum. Each SSM image has an error between $25{\cdot}10^{-3}$ and $65{\cdot}10^{-3}$ and the curve agrees well with the calculation. This proves the assumption that the error originates primarily from photon shot noise i.e. Poisson noise and no uncertainties from e.g. source instabilities occur.

Optics EXPRESS

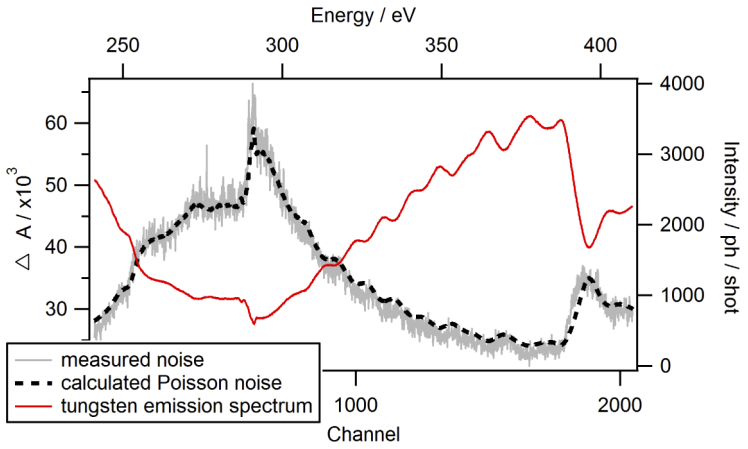

Fig. 5. The standard deviation derived from 500 SSM images yields the error of one single measurement. For this measurement the C K RZP was used in combination with the tungsten target. The measured standard deviation (grey) follows the calculated curve (black dash) which is derived by assuming Poisson noise as sole source or uncertainty.

This also simplifies the estimation of the needed SSM image number to achieve a specific value of certainty. On the CCD detector ~ 500–5000 photons per channel (10^4–10^5 ph/eV), depending on photon energy, filter transmission and laser pulse energy are detected per SSM image. For example at the C K-edge a $\Delta A(E)$ of $65{\cdot}10^{-3}$ was evaluated after data processing. This means averaging 1000 SSM images reduces the standard deviation of the NEXAFS spectrum to $65{\cdot}10^{-3}$ / $\sqrt{1000} = 2{\cdot}10^{-3}$. This is also confirmed by our investigations on TiO_2 (Ti L-edge and O K-edge spectra in Fig. 3 (top)). For example the Ti L-edge measurement yield a noise level of $3{\cdot}10^{-2}$ for the single shot NEXAFS. This value is reduced to $9{\cdot}10^{-4}$ which is $3{\cdot}10^{-2}/\sqrt{1500} + n_{ro}$. When measuring a sample this estimate has to be adjusted by the factor $\sqrt{e^A + 1}/\sqrt{2}$ caused by the increased absorption. For absorption values between 1 and 3 this is about 1.4 or 3.2 respectively. This multiplies the needed number of collected SSM spectra with a factor of 2 to 10 to reach the required certainty.

Figure 6 shows the needed number of SSM images to reach a certain value of $\Delta A(E)$ in a logarithmic scale. The black lines show the scenario with a photon number per channel and SSM images of 5000 and three different A values. A read out noise of $2{\cdot}10^{-4}$ is included as an offset in the calculation. A $\Delta A(E)$ of 10^{-3} is reached in a couple of thousand SSM images. The red curves show the case with only 500 photons. Thus a $\Delta A(E)$ of $< 10^{-3}$ can be reached within accumulating 20.000 SSM for most sample systems. Due to the limited read out rate of the CCD and switching speed of the pump beam shutter the data acquisition rate of our setup is currently limited to 1.5 Hz for NEXAFS and 0.4 Hz for pp-NEXAFS measurements. Because the LPP can run 24 hours a day autonomously about 34.000 SSM a day can be collected roughly reaching the CCD readout noise limit. If one could use the full 100 Hz of the system (e.g. by applying a high readout out rate sCMOS camera [38]) the same SNR could be accessible in only 6 minutes.

In pump probe spectroscopy the result is normally displayed as a difference spectrum $D_{pp}(E,t)$. The excited state spectrum $A_{pumped}(E,t)$ is subtracted from the ground state spectrum $A_{unpumped}(E)$.

$$D_{pp}(E,t) = A_{pumped}(E,t) - A_{unpumped}(E) \tag{4}$$

The error of the excited state spectrum and the ground state spectrum are basically the same if the number of SSM images is equal for both spectra. The error of the difference is therefore:

$$\Delta D_{pp}(E,t) = \sqrt{\Delta A^2_{pumped}(E,t) + \Delta A^2_{unpumped}(E)} \approx \sqrt{2} * \Delta A_{pumped}(E,t) \tag{5}$$

Optics EXPRESS

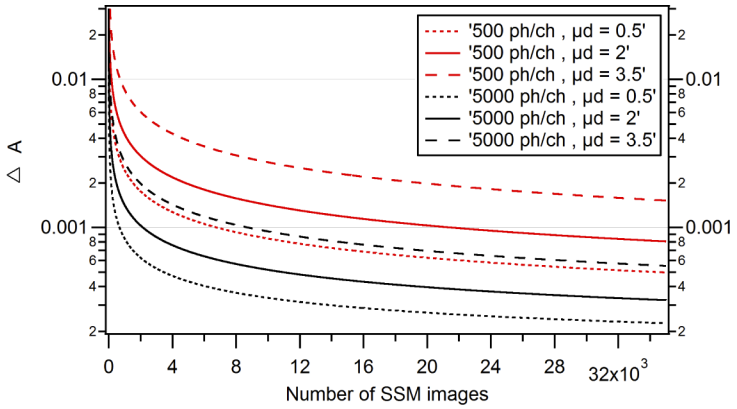

Fig. 6. The error ΔA of a NEXAFS spectrum independence on the number of averaged SSM images.

The stability of the source is high enough that it is even possible to evaluate only the sample spectra $S_{unpumped}(E,t)$ and $S_{pumped}(E,t)$ for the determination of $D_{pp}(E,t)$. Following the Lambert-Beer law the error of the difference can also be expressed with:

$$\Delta D_{pp}(E,t) = ln\sqrt{\frac{S_{unpumped}(E,t)}{S_{pumped}(E,t)}} \tag{6}$$

In that way the noise introduced by the reference spectrum is bypassed reducing the error of the difference by a factor of $\sqrt{2}$.

Figure 7 shows the difference of a blank measurement using the C K-edge RZP. As sample and reference a standard Si_3N_4 window was used. The difference between 4000 SSM images each was calculated. Shown here is only the difference of the sample spectra. The difference is clearly dependent on energy due to the varying brightness of the source. In the region from 275 to 325 eV the noise i.e. standard deviation of the difference spectrum is $1{\cdot}10^{-3}$ and in the region from 350 to 400 eV were the source is more bright, the noise is $5{\cdot}10^{-4}$.

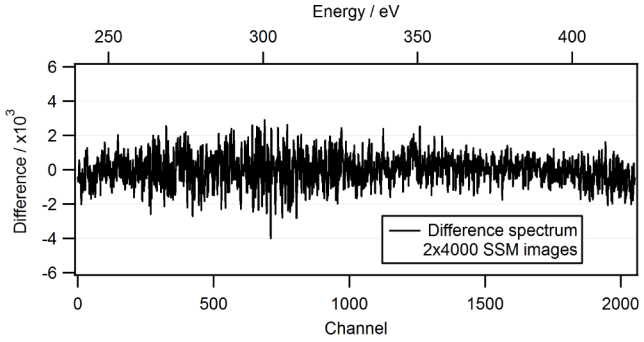

Fig. 7. The difference spectrum of 8000 SSM images measured with the C K RZP's is shown.

5. Discussion and Outlook

The presented setup consisting of a highly efficient and stable LPP source and an X- Ray absorption spectrometer shows the feasibility of utilizing table-top instrumentation for state-of-the-art X-ray

Optics EXPRESS

absorption spectroscopy with soft X-rays. The setup facilitates NEXAFS spectroscopy in the range between 284 eV and 1303 eV with a resolving power E/ΔE of up to 1370. The high efficiency and stability of the system are the prerequisites for the detection of minute changes in transient X-ray absorption. We have shown that dynamic differences in X-ray absorption down to 10^{-4} induced by optical pumping can be resolved rendering this setup suitable for a wide range of applications. Additionally, the possibility to measure absorption edges above 500 eV with high energy resolution makes this setup unique. First, the high average power laser with sub-ns pulse duration and the solid state target system guarantees high conversion efficiency from laser light to soft X-rays well beyond 1 keV. Second, the use of RZP optics in slit-less spectrometer geometry allow for high resolution single shot spectroscopy due to the utilization of a large collection angle compared to standard VLS spectrometers. And third, the high source stability due to shot to shot target correction mechanisms and simultaneous collection of sample and reference spectrum lead to the possibility for Poisson noise limited statistics.

The extension of the setup for simultaneous pp-NEXAFS measurement of two or more absorption edges with high resolution is possible, if an aperture is included in the setup. However in this case the throughput of the spectrometer is reduced by a factor of 5–10. The use of curved surfaces for the grating structures would be one option to eliminate this deficiency. Measurement times from a few seconds (C, N, O-edges) to hours (K-edges of Mg compounds or M-edges of rare earths compounds) are necessary for high quality spectra. Depending on the photon flux, two different modes (single shot and continuous) are available, which are mandatory because of the use of a conventional X-ray CCD detector. If 16-bit back illuminated sCMOS cameras with small pixel size and higher readout-speed become readily available and the 100 Hz signal of the source could be exploited, measurement times will be reduced drastically.

Funding

Deutsche Forschungsgemeinschaft (313838950); LASERLAB Europe (654148).

References

1. R. Geneaux, H. J. B. Marroux, A. Guggenmos, D. M. Neumark, and S. R. Leone, "Transient absorption spectroscopy using high harmonic generation: a review of ultrafast X-ray dynamics in molecules and solids," Phil. Trans. R. Soc. A **377**(2145), 20170463 (2019).
2. J. Weisshaupt, A. Rouzee, M. Woerner, M. J. J. Vrakking, T. Elsaesser, E. L. Shirley, and A. Borgschulte, "Ultrafast modulation of electronic structure by coherent phonon excitations," Phys. Rev. B **95**(8), 081101 (2017).
3. S. L. Cousin, F. Silva, S. Teichmann, M. Hemmer, B. Buades, and J. Biegert, "High-flux table-top soft x-ray source driven by sub-2-cycle,CEP stable, 1.85-µm 1kHz pulses for carbon K-edge spectroscopy," Opt. Lett. **39**(18), 5383–5386 (2014).
4. D. Popmintchev, B. R. Galloway, M.-C. Chen, F. Dollar, C. A. Mancuso, A. Hankla, L. Miaja-Avila, G. O'Neil, J. M. Shaw, G. Fan, S. Ališauskas, G. Andriukaitis, T. Balčiunas, O. D. Mücke, A. Pugzlys, A. Baltuška, H. C. Kapteyn, T. Popmintchev, and M. M. Murnane, "Near- and Extended-Edge X-Ray-Absorption Fine-Structure Spectroscopy Using Ultrafast Coherent High-Order Harmonic Supercontinua," Phys. Rev. Lett. **120**(9), 093002 (2018).
5. I. Mantouvalou, A. Jonas, K. Witte, R. Jung, H. Stiel, and B. Kanngießer, "Optimizing soft X-ray NEXAFS spectroscopy in the laboratory," Proc. SPIE **10243**, 1024308 (2017)..
6. P. Wachulak, M. Duda, A. Bartnik, A. Sarzyński, Ł Węgrzyński, M. Nowak, A. Jancarek, and H. Fiedorowicz, "Compact system for near edge X-ray fine structure (NEXAFS) spectroscopy using a laser-plasma light source," Opt. Express **26**(7), 8260–8274 (2018).
7. C. Peth, F. Barkusky, and K. Mann, "Near-edge x-ray absorption fine structure measurements using a laboratory-scale XUV source," J. Phys. D: Appl. Phys. **41**(10), 105202 (2008).
8. C. Kleine, M. Ekimova, G. Goldsztejn, S. Raabe, C. Strüber, J. Ludwig, S. Yarlagadda, S. Eisebitt, M. J. J. Vrakking, T. Elsaesser, E. T. J. Nibbering, and A. Rouzeé, "Soft X-ray Absorption Spectroscopy of Aqueous Solutions Using a Table-Top Femtosecond Soft X-ray Source," J. Phys. Chem. Lett. **10**(1), 52–58 (2019).
9. P. Grossmann, I. Rajkovic, R. Moré, J. Norpoth, S. Techert, C. Jooss, and K. Mann, "Time-resolved near-edge x-ray absorption fine structure spectroscopy on photo-induced phase transitions using a tabletop soft-x-ray spectrometer," Rev. Sci. Instrum. **83**(5), 053110 (2012).
10. P. Wachulak, M. Duda, A. Bartnik, Ł Węgrzyński, T. Fok, and H. Fiedorowicz, "NEXAFS at nitrogen K-edge and titanium L-edge using a laser-plasma soft –x-ray source based on a double-stream gas puff target," APL Photonics **4**(3), 030807 (2019).

Optics EXPRESS

11. C. Stamm, T. Kachel, N. Pontius, R. Mitzner, T. Quast, K. Holldack, S. Khan, C. Lupulescu, E. F. Aziz, M. Wietstruk, H. A. Durr, and W. Eberhardt, "Femtosecond modification of electron localization and transfer of angular momentum in nickel," Nat. Mater. **6**(10), 740–743 (2007).
12. C. Bressler, M. Saes, M. Cherugi, D. Grolimund, R. Abela, and P. Pattison, "Towards structural dynamics in condensed chemical systems exploiting ultrafast time-resolved x-ray absorption spectroscopy," J. Chem. Phys. **116**(7), 2955–2966 (2002).
13. F. Benesch, T. W. Lee, Y. Jiang, and C. G. Rose-Petruck, "Ultrafast laser-driven x-ray spectrometer for x-ray absorption spectroscopy of transition metal complexes," Opt. Lett. **29**(9), 1028–1030 (2004).
14. L. X. Chen, W. J. H. Jäger, J. Jennings, D. J. Gosztola, A. Munkholm, and J. P. Hessler, "Capturing a photoexcited molecular structure through time-domain X-ray absorption fine structure," Science **292**(5515), 262–264 (2001).
15. M. Ochmann, I. V. Ahnen, A. A. Cordones, A. Hussain, J. H. Lee, K. Hong, K. Adamczyk, O. Vendrell, T. K. Kim, R. W. Schoenlein, and N. Huse, "Light-induced radical formation and isomerization of an aromatic thiol in solution followed by time-resolved x-ray absorption spectroscopy at the sulfur K-edge," J. Am. Chem. Soc. **139**(13), 4797–4804 (2017).
16. H. Öström, H. Ölberg, H. Xin, J. LaRue, M. Beye, M. Dell'Angela, J. Gladh, M. L. Ng, J. A. Sellberg, S. Kaya, G. Mercurio, D. Nordlund, M. Hantschmann, F. Hieke, D. Kühn, W. F. Schlotter, G. L. Dakovski, J. J. Turner, M. P. Minitti, A. Mitra, S. P. Moeller, A. Föhlisch, M. Wolf, W. Wurth, M. Persson, J. K. Nørskov, F. Abild-Pedersen, H. Ogasawara, L. G. M. Petterson, and A. Nilsson, "Probing the transition state region in catalytic CO oxidation on Ru," Science **347**(6225), 978–982 (2015).
17. F. A. Lima, C. J. Milne, D. C. V. Amarasinghe, M. H. Rittmann-Frank, R. M. van der Veen, M. Reinhard, V. Pham, S. Karlsson, S. K. Johnson, D. Grolimund, C. Borca, T. Huthwelker, M. Janousch, F. v. Mourik, R. Abela, and M. Chergui, "A high-repetition rate scheme for synchrotron-based picosecond laser pump/x-ray probe experiments on chemical and biological systems in solution," Rev. Sci. Instrum. **82**(6), 063111 (2011).
18. M. W. Mara, D. N. Bowman, O. Buyukcakir, M. L. Shelby, K. Haldrup, J. Huang, M. R. Harpham, A. B. Stickrath, X. Thang, J. F. Stoddart, A. Coskun, E. Jakubikoa, and L. X. Chen, "Electron Injection from Copper Diimine Sensitizers into TiO_2: Structural Effects and Their Implications for Solar Energy Conversion Devices," J. Am. Chem. Soc. **137**(30), 9670–9684 (2015).
19. M. Fondell, S. Eckert, R. M. Jay, C. Weniger, W. Quevedo, J. Niskanen, B. Kennedy, F. Sorgenfrei, D. Schick, E. Giangrisostomi, R. Ovsyannikov, K. Adamczyk, N. Huse, P. Wernet, R. Mitzner, and A. Fohlisch, "Time-resolved soft X-ray absorption spectroscopy in transmission mode on liquids at MHz repetition rates," Struct. Dyn. **4**(5), 054902 (2017).
20. J. Mahl, S. Neppl, F. Roth, M. Borgwardt, C. Saladrigas, B. Toulson, J. Cooper, T. Rahman, H. Bluhm, J. Guo, W. Yang, N. Huse, W. Eberhardt, and O. Gessner, "Decomposing Electronic and Lattice Contributions in Optical Pump-X-ray Probe Transient Inner-Shell Absorption Spectroscopy of CuO," *Faraday Discuss.*, (2019)
21. T. J. A. Wolf, R. H. Myhre, J. P. Cryan, S. Coriani, R. J. Squibb, A. Battistoni, N. Berrah, C. Bostedt, P. Bucksbaum, G. Coslovich, R. Feilfe, K. J. Gaffney, J. Grilj, T. J. Martinez, S. Miyabe, S. P. moealler, M. Mucke, A. Natan, R. Obaid, T. Osipov, O. Plekan, S. Wang, H. Koch, and M. Gühr, "Probing ultrafast $\pi\ \pi^*$ /nπ^* internal conversion in organic chromophores via K-edge resonant absorption," Nat. Commun. **8**(1), 29 (2017).
22. H. Ito, T. Ito, N. Kurahashi, S. Thürmer, H. Tanaka, T. Katayama, T. Togashi, S. Owada, Y. Yamamoto, S. Karashima, J. Nishitani, M. Yabashi, T. Suzuki, and K. Misawa, "Femtosecond time-resolved X-ray absorption spectroscopy of anatase TiO_2 nanoparticles using XFEL," Struct. Dyn. **4**(4), 044033 (2017).
23. E. S. Ryland, M. Lin, M. A. Verkamp, K. Zhang, K. Benke, M. Carlson, and J. Vura-Weis, "Tabletop Femtosecond M-edge X-ray Absorption Near-Edge Structure of FeTPPCl: Metalloporphyrin Photophysics from the Perspective of the Metal," J. Am. Chem. Soc. **140**(13), 4691–4696 (2018).
24. A. Jonas, T. Meurer, B. Kanngießer, and I. Mantouvalou, "Note: Reflection zone plates as highly resolving broadband optics for soft X-ray laboratory spectrometers," Rev. Sci. Instrum. **89**(2), 026108 (2018).
25. I. Mantouvalou, K. Witte, D. Grötzsch, M. Neitzel, S. Günther, J. Baumann, R. Jung, H. Stiel, B. Kanngießer, and W. Sandner, "High average power, highly brilliant laser-produced plasma source for soft X-ray spectroscopy," Rev. Sci. Instrum. **86**(3), 035116 (2015).
26. I. Mantouvalou, R. Jung, J. Tuemmler, H. Legall, T. Bidu, H. Stiel, W. Malzer, B. Kanngießer, and W. Sandner, "Note: Study of extreme ultraviolet and soft x-ray emission of metal targets produced by laser-plasma-interaction," Rev. Sci. Instrum. **82**(6), 066103 (2011).
27. I. Mantouvalou, K. Witte, W. Martyanov, A. Jonas, D. Grötzsch, C. Streeck, H. Löchel, I. Rudolph, A. Erko, H. Stiel, and B. Kanngießer, "Single shot near edge x-ray absorption fine structure spectroscopy in the laboratory," Appl. Phys. Lett. **108**(20), 201106 (2016).
28. F. d. Groot, M. O. Figueiredo, M. J. Basto, M. Abbate, H. Peterson, and J. C. Fuggle, "2p X-ray absorption of titanium in minerals," Phys. Chem. Miner. **19**(3), 140–147 (1992).
29. G. S. Henderson, X. Liu, and M. E. Fleet, "A Ti L-edge X-ray absorption study of Ti-silicate glasses," Phys. Chem. Miner. **29**(1), 32–42 (2002).
30. J. P. Crocombette and F. Jollet, "Ti 2p X-ray absorption in titanium dioxides (TiO_2): the influence of the cation site environment," J. Phys.: Condens. Matter **6**(49), 10811–10821 (1994).
31. V. S. Lusvardi, M. A. Barteau, J. G. Chen, J. Eng Jr., B. Frühberger, and A. Teplyakov, "An NEXAFS investigation of the reduction and reoxidation of TiO_2(001)," Surf. Sci. **397**(1–3), 237–250 (1998).

Optics EXPRESS

32. F. M. F. de Groot, J. Faber, J. J. M. Michiels, M. T. Czyzyk, M. Abbate, and J. C. Fuggle, "Oxygen 1s x-ray absorption of tetravalent titanium oxides: A comparison with single-particle calculations," Phys. Rev. B **48**(4), 2074–2080 (1993).
33. M. Yoshiya, I. Tanaka, K. Kaneko, and H. Adachi, "First principles calculation of chemical shifts in ELNES/NEXAFS of titanium oxides," J. Phys.: Condens. Matter **11**(16), 3217–3228 (1999).
34. J. Guo, "Soft x-ray spectroscopy study of nanoscale materials," Proc. SPIE **5929**, 59290K (2005).
35. P. Jiang, D. Prendergast, F. Borondics, S. Porsgaard, L. Giovanetti, E. Pach, J. Newberg, H. Bluhm, F. Besenbacher, and M. Salmeron, "Experimental and theoretical investigation of the electronic structure of Cu_2O and CuO thin films on Cu(110) using x-ray photoelectron and absorption spectroscopy," J. Chem. Phys. **138**(2), 024704 (2013).
36. K. Witte, C. Streeck, I. Mantouvalou, S. A. Suchkova, H. Lokstein, D. Grötzsch, W. Martyanov, J. Weser, B. Kanngießer, B. Beckhoff, and H. Stiel, "Magnesium K-edge NEXAFS Spectroscopy of Chlorophyll a in Solution," J. Phys. Chem. B **120**(45), 11619–11627 (2016).
37. J. Baumann, R. Gnewkow, S. Staeck, V. Szwedowski-Rammert, C. Schlesiger, I. Mantouvalou, and B. Kanngießer, "Photon event evalutation for conventional pixelated detectors in energy-dispersive X-ray applications," J. Anal. At. Spectrom. **33**(12), 2043–2052 (2018).
38. K. Desjardins, H. Popescu, P. Mercère, C. Menneglier, R. Gaudemer, K. Thånell, and N. Jaouen, "Characterization of a back-illuminated CMOS camera for soft x-ray coherent scattering," AIP Conf. Proc. **2054**, 060066 (2019).